Article

Spatial Molecular AlO Temperature Distributions in Laser-Induced Plasma

David M. Surmick [1]*, Daryl J. Dagel[2] and Christian G. Parigger [3]

[1] University of Massachusetts of Lowell, 265 Riverside Street, Lowell, MA 01854;
[2] Sandia National Laboratories, 1515 Eubank, Albuquerque, NM 87115;
[3] Physics and Astronomy Department, University of Tennessee, University of Tennessee Space Institute, Center for Laser Applications, 411 B.H. Goethert Parkway, Tullahoma, TN 37388;
* Correspondence: david_surmick@uml.edu; Tel.: +1-978-934-3822

Abstract: Spatially resolved, line-of-sight measurements of aluminum monoxide emission spectra in laser ablation plasma are used with Abel inversion techniques to extract radial plasma temperatures. Contour mapping of the radially deconvolved signal intensity shows a ring of AlO formation near the plasma boundary with the ambient atmosphere. Simulations of the molecular spectra were coupled with the line profile fitting routines. Temperature results are presented with simultaneous inferences from lateral, asymmetric radial, and symmetric radial AlO spectral intensity profiles. This analysis indicates that we measured shockwave phenomena in the radial profiles, including a temperature drop behind the blast wave created during plasma initiation.

Keywords: Molecular Spectroscopy; Diatomic Spectroscopy; Abel Transform; Plasma Spectroscopy; Laser-Induced Breakdown Spectroscopy; Laser-Induced Plasma; Plasma Dynamics

1. Introduction

The act of tightly focusing laser radiation on to a target volume initiates plasma coupled with the propagation of a shockwave. Optical spectroscopy measurements of the dynamics are made in an effort to understand the chemistry kinetics of laser ablation plasma. Development of line-of-sight diagnostics for such systems are advantageous due to the numerous applications that are of interest, including scaling laws between high explosive events and laser-induced plasma shock, temperature, and electron density phenomena [1,2], molecular formation of nanocluster formation in laser plasma plumes [3], pulsed laser vapor deposition [4,5], and analytical applications of laser-induced breakdown spectroscopy (LIBS) [6,7]. In each of these applications the distribution of atomic and molecular emissions and the associated plasma state quantities, i.e., electron density and temperature, are of interest. In particular, correlations between spatial distributions molecular emission intensities and subsequent temperature inferences and the shock phenomena associated with laser-induced plasma are desirable. This information is most desirable for laser produced plasma at atmospheric conditions, as opposed to vacuum conditions, where the plasma and shock dynamics are more complex due to plume splitting, and confinement.

We consider asymmetric Abel inverted, diatomic molecular aluminum monoxide (AlO) emission spectra measured from laser produced plasma on the surface of an Al target sample in ambient laboratory air as a method for extracting further spatial distribution information about laser ablation plasma. Abel transformations and the more generalized Radon transformation relate lateral, line of sight measurements of the plasma emission intensity to the radial intensity distribution through well-known integral transformations [8,9]. This is done in an effort to extract information about the radial distributions of the molecular emission. Radon transformation techniques are commonly applied to laser ablation scenarios [10,11], however due to the more general nature of the Radon transformation, measurements made along multiple lines-of-sight are typically required. The Abel inversion assumes some type of symmetry, which alleviates the need for multiple line-of sight measurements. For a cylindrically symmetric emission source, the Abel transformation is given as

 doi:10.20944/preprints201907.0156.v1

$$I(z,\lambda) = 2\int_r^R I(r,\lambda)\frac{rdr}{\sqrt{r^2-z^2}}. \quad (1)$$

Here, $I(z,\lambda)$ is the lateral spectral measurement and $I(r,\lambda)$ is the radial reconstruction. The upper limit of the integral, R , is often carried out to be much greater than the extent of the plasma. The integral pre-factor of 2 indicates the plasma symmetry along the radial and lateral axes.

The desire in attempting to apply Abel reconstructions over the Radon deconvolutional methods is to adopt a procedure that is more widely applicable given the ease with which a single lateral, spectral measurement can be made along a single axis of the plasma plume. Further, numeric methods for implementing Abel transformation are plenty and can be applied with little computational expense. Asymmetries are included by using a procedure developed by Blades [12], originally applied to inductively coupled plasma with slightly asymmetric spectral emissions. This method focusses on the creation of a symmetric profile from two plasma emission halves that are symmetric, yet show different symmetries. Particular to laser-induced plasma, algorithmic implementations of asymmetric Abel inversions exist [13–15], in which the emission intensity is decomposed into symmetric and asymmetric components. The method of asymmetric inclusion for this work is selected for the relative ease with which the method can be implemented. Consequences of applying the asymmetric Abel inversions are considered for application of inferring the plasma temperature from the measured, lateral AlO emission profiles.

2. Experiment

Spectra were collected following laser-induced breakdown initiated in ambient laboratory air using a Quantel Ultra Light Q-switched Nd:YAG laser with a pulse width of 8.5 ns, as measured by a fast silicon photodiode. The laser operated at the fundamental wavelength of 1064 nm with an average energy per pulse of 38 mJ at the ablation site. The ablation target was the narrow edge of 5 cm square aluminum alloy 6061 sheet that was approximately 1 mm thick. The AlO spectra are imaged onto the slit of a Princeton instruments Isoplane SCT 320 spectrometer installed with an 1800 grooves/mm grating and a focal length of 0.33 meters. Spatially and temporally resolved spectral images of the ablation event were recorded using a Princeton Instruments PiMax2 ICCD. The ICCD had a pixel arrangement of 256x10245 vertical by horizontal pixels. The horizontal axis was used to achieve the desired spectral resolution and the vertical axis was used to achieve spatial resolution along the plasma plume expansion height. Groups of 2 vertical pixels were binned together in order to improve the signal quality of the AlO emissions with respect to the measurement noise. The detector pixel size is 25μm square such that in the binned configuration the effective pixel size was 50x25 μm. The imaging of the spectrometer-detector arrangement is such that the breakdown plasma is magnified at a ratio of 1:1.8. The was determined using a negative of the 1951 USAF target. The spectral resolution of the spectrometer-detector arrangement was approximately 0.1 nm in the spectral region between 480 to 500 nm. The spectra used for analysis were the result of 100 accumulations on a single ablation site. The spectrometer-detector arrangement was calibrated for the system wavelength response using a Hg/Ne-Ar lamp and the system intensity response using a tungsten lamp with a known spectral intensity response curve. Time synchronization of the system was achieved by synchronizing the ICCD gate opening to the Q-switch of the laser.

3. Results and Discussion

Figure 1 shows contour mappings of spatially resolved measurements of AlO spectra between time delays of 20 and 35 μs following optical breakdown along the axis of laser incidence. The ablation surface is located at a slit height of 1.0 mm. Here we note that slit height units refer to the image plane measurement and not the exact positions of the spectral emissions in the plasma. Detailed ray tracings of the spectral imaging system (non trivial) would be required to correlate image plane units to the plasma emission source. Initially the AlO signal intensity is relatively isotropic between slit heights of

Preprints (www.preprints.org) | NOT PEER-REVIEWED | Posted: 11 July 2019 doi:10.20944/preprints201907.0156.v1

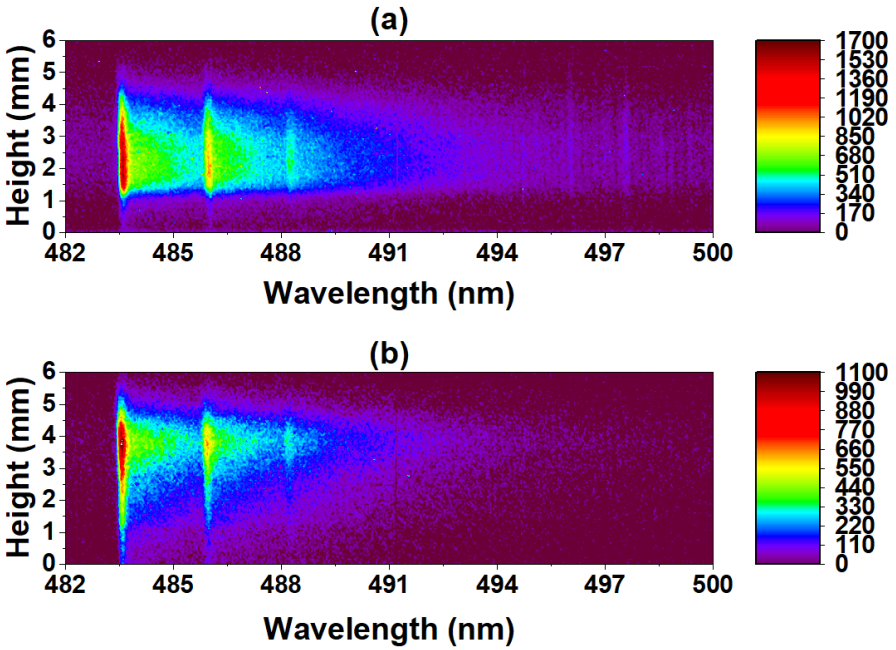

Figure 1. Contour mappings of spatially resolved AlO spectral measurements along the plasma plume height measured at (a) 20 μs and (b) 35 μs time delays.

1.5 and 3.5 mm (Fig.1a). As the time delay increases, the spectroscopic intensity is seen to diminish, which is roughly correlated with the decay of the laser-induced plasma. As the time delay increases, areas of larger AlO signal intensity farther from the ablation surface, see 3.5 to 4 mm slit heights in Fig1(b). These areas of increased intensity also appear to be asymmetric, with stronger emissions occurring in the higher half of the plume, which is also the direction of the plasma plume and plasma formation blast wave propagation. The asymmetry of the axial, spectroscopic lines-of-sight likely indicates asymmetries in the radial profiles of the AlO emissions and the need for an asymmetric Abel deconvolution.

The radial intensity distribution of plasma emissions are extracted through application of the Abel inversion under the assumption of cylindrical symmetry. Under such a scenario the Abel inverse transform is given by

$$I(r,\lambda) = \frac{-1}{\pi}\int_r^R \frac{dI(z,\lambda)}{dz}\frac{dz}{\sqrt{z^2-r^2}}, \tag{2}$$

where z is the lateral coordinate along the light of sight, r is the radial coordinate, $I(z,\lambda)$ is the line of sight measurement, and $I(r,\lambda)$ is the deconvolved radial intensity profile.

In order to obtain an Abel inversion that accounts for minor asymmetries in the plasma spectral emissions, we consider the procedure introduced by Blades, in which Abel inversion symmetry is assigned to upper and lower plasma spectral regions [12]. These two regions are used to generate a symmetric intensity profile,

$$I_0(z,\lambda) = \frac{I(+z,\lambda) + I(-z,\lambda)}{2} \tag{3}$$

by averaging the upper and lower plasma regions. The total inverted profile is given by

$$I(\pm r,\lambda) = G(\pm z,\lambda) I_0(r,\lambda) \tag{4}$$

where $I_0(r,\lambda)$ is the Abel inversion of $I_0(z,\lambda)$ and $G(\pm z,\lambda)$ is given by

Preprints (www.preprints.org) | NOT PEER-REVIEWED | Posted: 11 July 2019 doi:10.20944/preprints201907.0156.v1

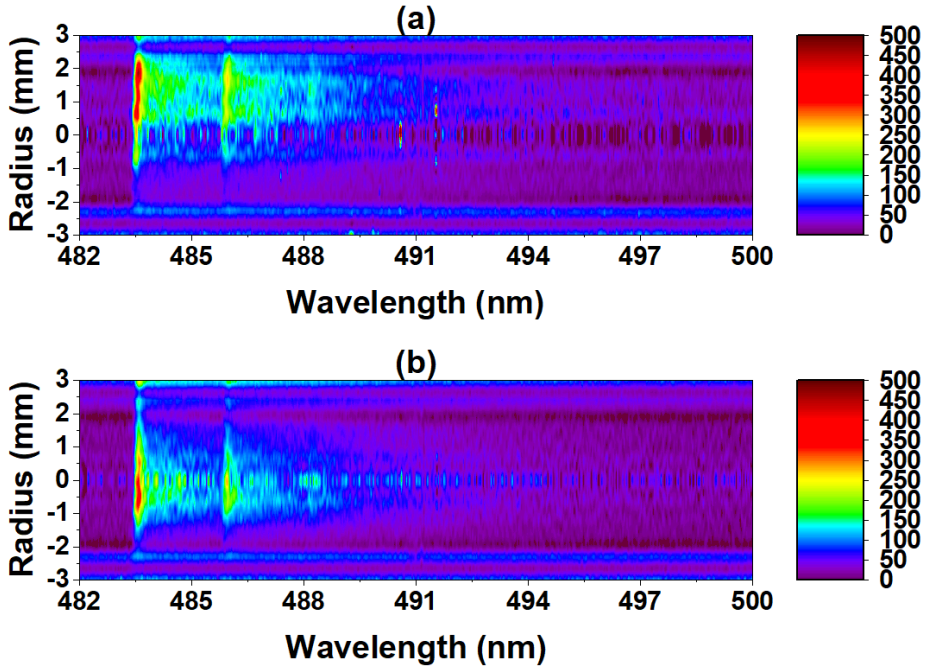

Figure 2. Contour mappings of extracted radial deconvolutions of measured AlO spectra at (a) 20 μs and (b) 35 μs time delays.

$$G(\pm z, \lambda) = \frac{I(\pm z, \lambda)}{I_0(r, \lambda)}. \tag{5}$$

This factor accounts for difference between the upper and lower half plasma regions and the symmetrized axial intensity distribution.

Application of the above procedure was carried out on the emission spectra depicted in the spectral contour mappings presented in Figure 1. The results of the asymmetric Abel inversion are presented in spatial-spectral contour maps in Figure 2. The method by which the Abel inversion of the symmetrized axial profile represented by Equation 2 uses a series expansion of orthogonal polynomials in which series expansion coefficients are determined through minimization techniques [16]. The orthogonal set of polynomials is taken to be Chebyshev polynomials of the first kind. The number of terms to be used in the procedure is 10. This maintains a decent fidelity of the deconvolved profile while avoiding potential oscillatory behavior and noise addition by considering significantly more series terms. The advantage of such a method is it alleviates the need to numerically compute the derivative presented in Equation 1 by way of the series expansion approximation. Such advantages exist in other Abel inversion implementations as well [17]. The Abel inversion is performed through use of a formalized MatLab script [18].

The largest source of error in the deconvultion procedure results from considering too small of a radius or applying the deconvlution to too small of an axial region. Attempting to apply the deconvultion procedure with a smaller axial region than the plasma radius will result in an inflated deconvolved signal intensity. By considering a smaller region of the plasma, oscillatory behavior from the Abel inversion algorithm becomes prevalent in the radial profile. Also, edge effects tend to occur, whereby the radial deconvlution tends toward arbitrarily large values for the largest radius values in the deconvolution. Given the limitations in the size of an ICCD detector vs. the plasma image size, some of these effects may not be completely overcome in the outlined procedure. These effects were reduced in magnitude by applying the deconvolution procedure over most of the detector height,

Preprints (www.preprints.org) | NOT PEER-REVIEWED | Posted: 11 July 2019 doi:10.20944/preprints201907.0156.v1

using slit heights from 0 to 6 mm. This was done since the AlO emission intensities are centered about a slit height of 3 mm. The calculated radial profiles correspond with this axial position.

The noisy nature of the deconvolution procedure is evident in the contour images of Figure 2, which is depicted by the fuzziness of the images. Potential edge effects are also apparent in each of the spectroscopic contour mappings and each favor a particular radial direction. Namely, the positive radial direction are favored. The positive direction corresponds to contributions from the lower plasma region. Reductions in quality of the deconvolution in this direction occur due to the presence of the aluminum surface.

Temperatures are determined from the molecular AlO emissions by fitting simulated AlO spectra to the line of sight measurements and radially deconvolved spectra. The theory spectra are simulated by making use of accurately complied tables of line strengths for the diatomic molecule of interest [19]. In short, the intensity of a measured molecular line from upper state, u, to lower state, l, is given by

$$I_{ul} = \frac{16\pi^3 c(a_0 e)^2 C_{abs} N_0}{3\epsilon_0 Q} C_\nu \nu_u l^4 S_{ul} e^{hF_u/kT} \tag{6}$$

where a_0 is the Bohr radius, e, is the electronic charge, c is the speed of light, Q is the partition function, N_0 is the total population of the species, C_{abs} and C_ν are the absolute and relative calibration factors, h is Planck's constant, F_u is the upper term value, k is Boltzmann's constant, and T is the temperature. The term S_{ul} is the diatomic line strength and is calculated in a factorized form to account for electronic, vibrational, and rotational molecular structure. Detailed procedures for calculating a spectrum from the diatomic line strength are outlined in References [20–22].

Given the temperature dependence of the molecular spectrum, a fitting routine was used to extract the temperature of each temporally and spatially resolved AlO spectrum. Fitting was performed using a Trust-Region fitting routine with fitting parameters of temperature, line amplitude, and linear offset [23,24]. Additionally, the spectral resolution is a variable parameter that is used to establish the uncertainty of the inferred temperature from diatomic line profile fitting. Following initial fitting of each spectrum, the linear offset and spectral resolution parameters were randomly varied 1000 times and subsequently re-fit to generate a distribution of possible temperatures for each AlO spectrum. An additional fit was performed in which the line amplitude, temperature, linear offset, and spectral resolution were fit parameters. A total 1002 inferred temperatures were used to establish 1-σ uncertainties according to the so-called Three Sigma Rule (68-95-99 Rule) for Gaussian distirbutions[25].

Figures 3 and 4 show calculated temperatures both in the lateral direction on the plasma plume height and in the deconvolved radial directions for 20 μs and 35 μs time delay following plasma initiation, respectively. These times were chosen to illustrate the different behaviors of the plasma expansions at two time delays that were as distinct as possible from each other. For the sake of validity of application of the asymmetric Abel inversion method to molecular emissions in laser ablation plasma, temperature inferences in which a symmetric Abel inversion was calculated are also presented. The shaded region surrounding the symmetric Abel deconvolution (red dashed line) in Figures 3 and 4 represents the uncertainty of this temperature inference.

The axial temperatures at both 20, Fig. 3(b) and 35, Fig. 4(b) μs do not show much structure beyond the calculated 1-σ uncertainties and show relatively constant temperatures of approximately 3400 and 3100 K, respectively, when averaging along the radial and axial directions. The displayed spectra and spatial temperature expansions of central part of the plume. The spatial temperature distributions along the axial coordinates in Figs. 3(b) and (4(b) indicate slightly higher temperatures near the boundaries, especially away from the target indicating the remnants of the laser-driven plasma excitation. Similarly, Figs. 3(a) and 3(b) reveal slightly higher temperature near the edges, and with larger variation away from the target as indicated by the asymmetric results. The larger uncertainties in the negative radial directions correspond to weaker AlO signals in the upper most regions of the spatially resolved measurement (see Fig. 1). The axial temperature expansion of the AlO molecules is

Preprints (www.preprints.org) | NOT PEER-REVIEWED | Posted: 11 July 2019 doi:10.20944/preprints201907.0156.v1

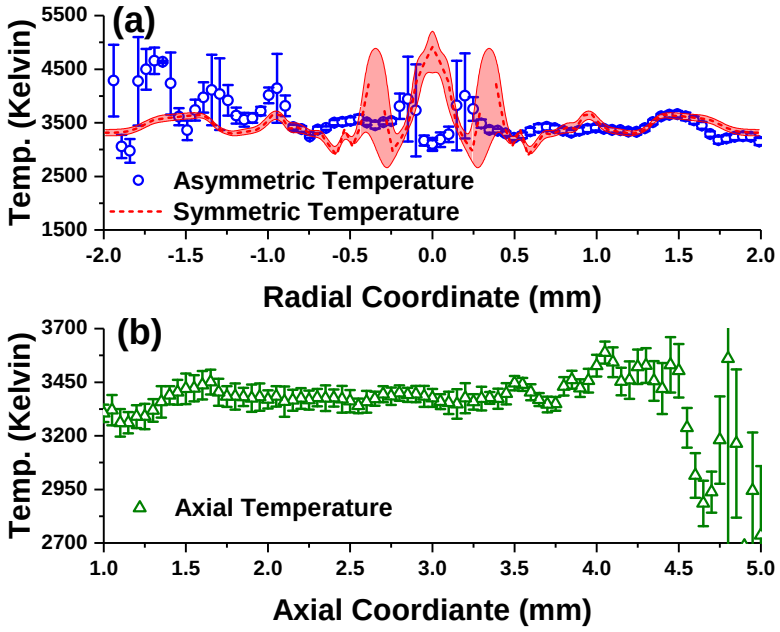

Figure 3. Temperatures inferred from AlO spectra at a time delay of 20 μs following ablation (a) along the plasma radius using asymmetric and symmetric Abel inverted spectra and (b) along the plasma using spatially resolved line-of-sight spectral measurements.

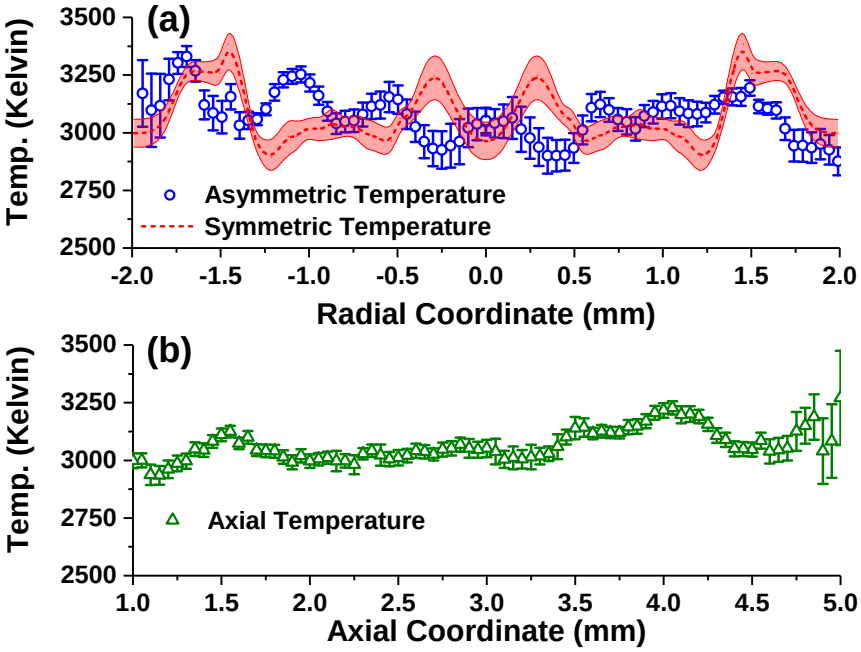

Figure 4. Temperatures inferred from AlO spectra at a time delay of 35 μs following ablation (a) along the plasma radius using asymmetric and symmetric Abel inverted spectra and (b) along the plasma using spatially resolved line-of-sight spectral measurements.

of the order of 80 to 100 m/s, but the radial expansion appears to occur at lower speeds towards the plasma center.

For nominal 100 mJ, 10 ns pulsed laser radiation, the shock wave expands at speeds of the order of 1 mm/μs or 1000 m/s (Ma=3) at 1 μs time delay. For 38 mJ pulses the shock wave radius will be smaller according to the Taylor-Sedov blast wave model [26,27]. Moreover, for the investigated time delays of 20 and 35 μs, the Taylor-Sedov blast wave model predicts a shock wave radius of 2.7 and

 doi:10.20944/preprints201907.0156.v1

3.4 mm, respectively, moving at speeds approaching the speed of sound (Ma=1). Therefore, the axial temperature profiles show in part, the effects of the shock wave, indicated near 2.5 mm from center (or at the abscissa of 5 mm) in Fig. 3(b), but the shock wave appears to be just outside the investigated axial position in Fig 4(b). Consequently, a temperature drop near the shock wave from about 3300 K to 2800 K (see Fig. 3 (b)) is quite reasonable. The radial profiles also indicate, in part, the shock wave effects near 2 mm. Moreover, it would not be unexpected to see an elevated temperature of AlO just inside the shock wave, with a slight indication of smaller temperatures at center.

4. Conclusions

In summary, we have shown that asymmetric Abel deconvolutional methods can be applied to obtain spatial information of molecular spectra in laser ablation plasma plumes. When coupled with diatomic line profile fitting of AlO emissions, we were able to demonstrate the impact of the propagating shockwave has on the plasma state in both radial and axial directions. Namely, multiple temperature gradients exist which correspond to the leading/following edges of the plasma blast wave. Further insight into the shockwave interaction with the plasma material may obtained by coupling the radial deconvolution analysis with shockwave imaging studies, such as shadowgraph or schlieren techniques, or interferometric methods [28,29]. The purpose of such a study would be to elucidate the affect of the plasma shockwave on the chemical kinetics of the plasma plume expansion into ambient atmospheres.

Author Contributions: All authors contributed equally to this work.

Funding: This paper describes objective technical results and analysis. Any subjective views or opinions that might be expressed in the paper do not necessarily represent the views of the U.S. Department of Energy or the United States Government. Sandia National Laboratories is a multimission laboratory managed and operated by National Technology and Engineering Solutions of Sandia, LLC., a wholly owned subsidiary of Honeywell International, Inc., for the U.S. Department of Energy's National Nuclear Security Administration under contract DE-NA0003525

Conflicts of Interest: The authors declare no conflict of interest.

References

1. Kimblin, C.; Trainahm, R.; Capelle, G.; Mao, X.; Russo, R. LIBS as a compliment to large-scale detonations and means to characterize intermediates. Technical report, Special Technologies Laboratory, LLC, Las Vegas, NV, 2015.
2. Kimblin, C.; Trainham, R.; Capelle, G.; Mao, X.; Russo, R. LIBS as a surrogate for large-scale detonations and means to characterize intermediates. Technical report, Special Technologies Laboratory, LLC, Las Vegas, NV, 2014.
3. Harilal, S.; Brumfield, B.; Cannon, B.; Phillips, M. Shock wave mediated plume chemistry for molecular formation in laser ablation plasmas. *Anal. Chem.* **2016**, *88*, 2296–2302.
4. Singh, R.K.; Narayan, J. Pulsed-laser evaporation technique for deposition of thin films: Physics and theoretical model. *Phys. Rev. B* **1990**, *41*, 8843–8859.
5. Panda, A.K.; Singh, A.; Thirumurugesan, R.; Kuppusami, P.; Mohandas, E. Optimization of substrate-target distance for pulsed laser deposition of tungsten oxide thin films using Langmuir probe. *J. Instrum.* **2015**, *10*, P09014.
6. Hahn, D.; Omenetto, N. Laser-Induced Breakdown Spectroscopy (LIBS), Part 1: Review of Basic Diagnostics and Plasma-Paritcle Interactions: Still-Challeneging Issues Within the Analytical Plasma Community. *Appl. Spectrosc.* **2010**, *64*, 335A–366A.
7. Tognoni, E.; Cristoforetti, G.; Legnaioli, S.; Palleschi, V. Calibration-Free Laser-Induced Breakdown Spectroscopy: State of the art. *Spectrochim. Acta Part B: At. Spectrosc.* **2010**, *65*, 1 – 14.
8. Kunze, H.-J. *Introduction to Plasma Spectroscopy*; Springer-Verlag: Berlin, Heidelberg, 2009.
9. Deans, S. *The Radon transform and some of its applications*; John Wiley and Sons: New York, 1983.

10. Gornushkin, I.; Merk, S.; Demidov, A.; Panne, U.; Shabanov, S.; Smith, B.; Omenetto, N. Tomography of single and double pulse laser-induced plasma using radon transform technique. *Spectrochim. Act. Part B: At. Spectrosc.* **2012**, *76*, 203–213.
11. Eschlböck-Fuchs, S.; Demidov, A.; Gornushkin, I.; Schmid, T.; Rössler, R.; Huber, N.; Panne, U.; Pedarnig, J. Tomography of homogenized laser-induced plasma by Radon transform technique. *Spectrochim. Acta Part B: At. Spectrosc.* **2016**, *123*, 59 – 67.
12. Blades, M. Asymmetric abel inversions on inductively coupled plasma spatial emission profiles collected from a photdiode array. *Appl. Spectrosc.* **1983**, *37*, 371–375.
13. Tomassini, P.; Giulietti, A. A generalization of Abel inversion to non-axisymmetric density distribution. *Opt. Commun.* **2001**, *199*, 143 – 148.
14. Cristoforetti, G.; Legnaioli, S.; Palleschi, V.; Salvetti, A.; Tognoni, E.; Tomassini, P. Reconstruction of laser-induced plasma spectral emissivity in non-axisymmetric conditions. *Spectrochim. Acta Part B: At. Spectrosc.* **2005**, *60*, 888 – 896.
15. Wetzer, J.M. Asymmetrical Abel Inversion of MHD Generator Discharges. *IEEE Transactions on Plasma Science* **1983**, *11*, 72–75.
16. Pretzler, G. A new method for numerical abel-inversion. *Z. Naturforsch.* **1991**, *46a*, 639–641.
17. Aguilera, J.; Benegoechea, J.; Aragon, C. Curves of growth of spectral lines emitted by a laser-induced plasma: Influence of the temporal evolution and spatial inhomogeneity of the plamsa. *Spechtrochim. Act. B* **2003**, *58*, 221–237.
18. Killer, C. http://www.mathworks.com/matlabcentral/fileexchange/43639-abel-inversion-algorithm, [accessed Nov 15 2015], 2014.
19. Parigger, C.G.; Hornkohl, J.O. Computation of AlO $B^2\Sigma^+ \rightarrow X^2\Sigma^+$ emission spectra. *Spectrochim. Acta Part A: Mol. Biomol. Spectrosc.* **2011**, *81*, 404 – 411. doi:http://dx.doi.org/10.1016/j.saa.2011.06.029.
20. Parigger, C.G.; Woods, A.C.; Surmick, D.M.; Gautam, G.; Witte, M.J.; Hornkohl, J.O. Computation of diatomic molecular spectra for selected transitions of aluminum monoxide, cyanide, diatomic carbon, and titanium monoxide. *Spectrochim. Acta Part B: At. Spectrosc.* **2015**, *107*, 132 – 138.
21. Woods, A.; Parigger, C.; Hornkohl, J. Measurement and analysis of titanium monoxide spetra in laser-induced plasma. *Opt. Lett.* **2012**, *37*, 5139–5141.
22. Surmick, D.M.; Parigger, C.G. Aluminum Monoxide Emission Measurements in a Laser-Induced Plasma. *Appl. Spectrosc.* **2014**, *68*, 992–996. doi:10.1366/13-07379.
23. Byrd, R.; Schnabel, R.; Schultz, G. A trust region algorithm for nonlinearly constrained optimization. *SIAM J. Numer. Anal.* **1987**, *24*, 1152–1170.
24. Sorenson, D. Newton's method with a model trust region modification. *SIAM J. Numer. Anal.* **1982**, *19*, 409–426.
25. Pukelscheim, F. The Three Sigma Rule. *American Statistician* **1994**, *48*, 88–91.
26. Sedov, L. *Similarity and dimensional methods in mechanics*, second ed.; Academic Press: New York, 1959.
27. Taylor, G. The formation of a blastwave by a very intense explosion. *Proc. R. Soc. London Ser. A* **1950**, *201*, 159–174.
28. Hough, P.; Kelly, T.J.; Fallon, C.; McLoughlin, C.; Hayden, P.; Kennedy, E.T.; Mosnier, J.P.; Harilal, S.S.; Costello, J.T. Enhanced shock wave detection sensitivity for laser-produced plasmas in low pressure ambient gases using interferometry. *Meas. Sci. Technol.* **2012**, *23*, 125204.
29. Harilal, S.; Milshevsky, G.; Diwakar, P.; LaHaye, N.; Hassanein, A. Experimental and computational study of complex shockwave dynamics in laser ablation plumes in argon atmospheres. *Phys. Plasmas* **2012**, *19*, 083504:1–11.